

## Negative and positive electroluminescence from a compensated p-type germanium in terahertz frequencies

P. K. Chung, J. M. Lin, S. T. Yen, and T. H. Wang

Citation: [Applied Physics Letters](#) **91**, 241106 (2007); doi: 10.1063/1.2824577

View online: <http://dx.doi.org/10.1063/1.2824577>

View Table of Contents: <http://scitation.aip.org/content/aip/journal/apl/91/24?ver=pdfcov>

Published by the [AIP Publishing](#)

---

### Articles you may be interested in

[Fine structure and hyperfine perturbations in the pure rotational spectrum of the VCl radical in its  \$X^5r\$  state](#)  
J. Chem. Phys. **130**, 164301 (2009); 10.1063/1.3108538

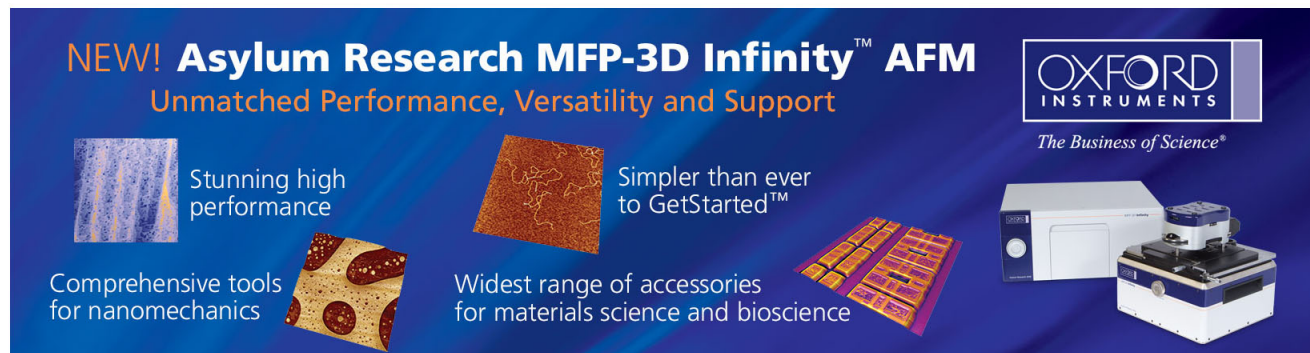
[Internal voltages in Ga In P Ga In As Ge multijunction solar cells determined by electroluminescence measurements](#)  
Appl. Phys. Lett. **92**, 123502 (2008); 10.1063/1.2903101

[Germanium n-type shallow junction activation dependences](#)  
Appl. Phys. Lett. **87**, 091909 (2005); 10.1063/1.2037861

[Room-temperature electroluminescence at 1.3 and 1.5  \$\mu\text{m}\$  from Ge/Si self-assembled quantum dots](#)  
Appl. Phys. Lett. **83**, 2958 (2003); 10.1063/1.1616665

[The pure rotational spectrum of CaNH 2 and CaND 2 \( \$X^2A\_1\$ \): Additional proof of planarity](#)  
J. Chem. Phys. **113**, 3141 (2000); 10.1063/1.1286919

---

The advertisement features a dark blue background with white and orange text. At the top left, it reads 'NEW! Asylum Research MFP-3D Infinity™ AFM' in large white letters, with 'Unmatched Performance, Versatility and Support' in orange below it. To the right is the Oxford Instruments logo, which includes the text 'OXFORD INSTRUMENTS' and the tagline 'The Business of Science®'. Below the main text are four images: a blue textured surface, a brown textured surface, a grid of colorful squares, and a photograph of the AFM instrument. Each image is accompanied by a short text description: 'Stunning high performance', 'Simpler than ever to GetStarted™', 'Comprehensive tools for nanomechanics', and 'Widest range of accessories for materials science and bioscience'.

## Negative and positive electroluminescence from a compensated *p*-type germanium in terahertz frequencies

P. K. Chung, J. M. Lin, S. T. Yen,<sup>a)</sup> and T. H. Wang

Department of Electronics Engineering, National Chiao Tung University, Hsinchu, Taiwan 30050, Republic of China

(Received 7 September 2007; accepted 26 November 2007; published online 12 December 2007)

Negative luminescence (NL) and positive luminescence in terahertz frequencies were observed from a compensated *p*-type Ge under various levels of pulse excitations at cryogenic temperatures. The NL spectra accompanying an *S*-type negative differential resistance phenomenon were attributed to the reduced emission transitions from the excited states to the ground states of the acceptors during the excitation. A possible excitation mechanism is also presented according to the measured data.

© 2007 American Institute of Physics. [DOI: 10.1063/1.2824577]

Terahertz frequencies (usually in 1–10 THz) lie between two electromagnetic spectral regions with quite matured theories and applications. In recent years, lots of efforts have been put in to unveil the terahertz physics and discover their potential uses. Finding low cost, compact, and efficient terahertz emitters and detectors is important since most of the gas molecules and chemicals have their fingerprints inside the terahertz frequencies. Terahertz imaging techniques have been used not only for biomedical but also for security reasons.<sup>1,2</sup> Quantum cascade lasers<sup>3</sup> and emitters<sup>4</sup> made from III-V compounds and SiGe have drawn lots of attention in the past few years. Terahertz waves can also be generated from level-to-level transitions of shallow impurity centers (*n*- or *p*-type) in semiconductors (Si or Ge) at low temperature. These hydrogenic centers have their level spacings naturally in the terahertz region.<sup>5</sup> Optical pumping of *n*-type silicon by CO<sub>2</sub> lasers can even cause terahertz lasing.<sup>6</sup> The research on electrical pumping of *n*- and *p*-type semiconductors for producing terahertz emission has regained its popularity in recent years.<sup>7,8</sup> However, not much attention<sup>9</sup> has been paid to the emission characteristics of compensated semiconductors (i.e., doped simultaneously with donors and acceptors).

In this work, we investigate the emission signals and spectra in the terahertz range from a lightly doped compensated *p*-type Ge under different levels of electrical pulses at cryogenic temperatures. The emission signals show obvious negative luminescence (NL) as well as conventional positive luminescence (PL). The NL phenomenon has been observed in the infrared range from narrow-gap semiconductors, including Ge, through magnetoconcentration effect and carrier extraction from *p*-*n* junctions at room temperature and above.<sup>10</sup> Under such circumstances, the emission from interband transition is suppressed and the samples are out of equilibrium with their enclosures. The radiation emitted from the samples is thus less in intensity than that absorbed by the samples. The NL property can be applied not only to radiation detection but also to radiation shielding or cooling.<sup>11</sup>

A one-side-polished compensated *p*-type Ge:Ga sample having dimensions of 5.05 × 4.3 × 1.98 mm<sup>3</sup> was attached to a copper heat sink by GE varnish and then mounted on a cryostat cold finger. The sample has a net dopant concentration of  $N_A - N_D \approx 2 \times 10^{14}$  cm<sup>-3</sup> and a compensation ratio of

$N_D/N_A \geq 0.01$ , estimated respectively from the room-temperature conductivity of 13 Ω cm and the breakdown field of 4.2 V/cm at 4.2 K.<sup>12</sup> The cryostat was equipped with cold white inner PE windows and a radiation shield to prevent the interference of room-temperature background radiation. Voltage pulses, with widths of 1.05 and 2.1 ms and a repetition rate of 157 Hz, were applied. Current was monitored on an oscilloscope by measuring the voltage across a 10 Ω resistor in series with the sample. A thermal resistor was placed adjacent to the sample to record the temperature. Emission spectra from the polished surface (5.05 × 4.3 mm<sup>2</sup>) were measured by a Bruker IFS 66v/s Fourier transform infrared spectrometer using the step-scan amplitude modulation technique with an SR850 lock-in amplifier (LIA). A Mylar beam splitter, outer white PE windows (on the cryostat), and a silicon bolometer were used for far infrared emission detection (with a detectable range from about 20 to 700 cm<sup>-1</sup>).

Figure 1 shows the variations of the electric field  $E$  and the conductivity  $\sigma$  in (a) and the integrated emission intensity  $I$  in (b) with the current density  $J$ . The temperature measured is slightly increased with  $J$  from 8 to 12 K. The *S*-type negative differential resistance (SNDR) phenomenon, one of the characteristics of heavily compensated Ge,<sup>13,14</sup> can be clearly seen from the  $E$ - $J$  curves in Fig. 1(a) under low current excitation. It is found that the SNDR occurs only at low enough temperature (<10 K) and the transition of the  $E$ - $J$  curve from the SNDR to the Ohmic region depends on the pulse width. The SNDR is less obvious for narrower pulses because of the shorter time for ionization to produce free carriers. Furthermore, the reduction of  $E$  with  $J$  indicates a superlinear increase of  $\sigma$ , revealing also a superlinear increase of the free hole concentration  $p$  in the SNDR region. It is believed that these free carriers come mainly from the preoccupied excited states, instead of the ground states, due to the larger impact ionization coefficient.<sup>14,15</sup> The emission intensity in Fig. 1(b) is obtained by reading the LIA output at the center peak of the interferograms and is further checked with the detector facing the emission sample directly. It can be seen that there appear two peaks for each  $I$ - $J$  curve; the first peak position corresponds to the local minimum of  $E$  (the end of the SNDR region), while the second one to the maximum of  $\sigma$ . The positions of both the peaks shift toward higher  $J$  as the pulse width is reduced from 2.1 to 1.05 ms.

<sup>a)</sup>Electronic mail: styen@faculty.nctu.edu.tw

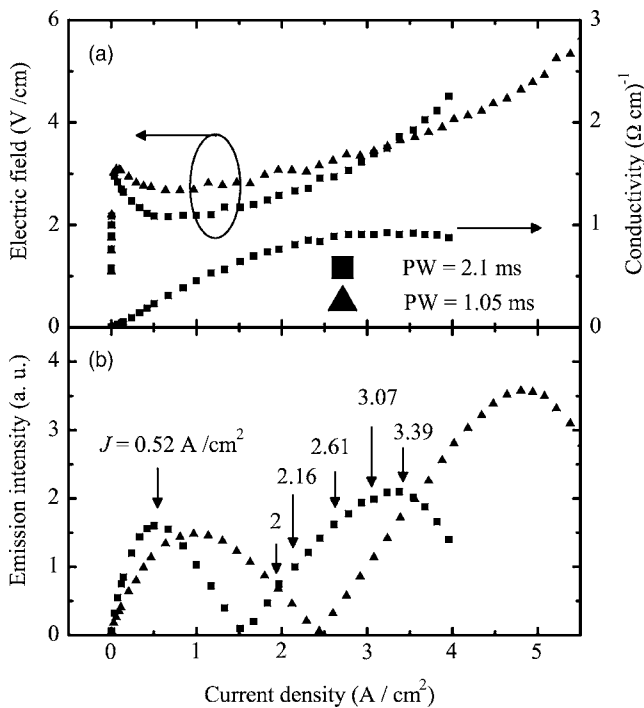


FIG. 1. Dependence of the electric field and the conductivity in (a) and the emission intensity in (b) on the current density for the sample under excitation pulses with widths of 1.05 and 2.1 ms and a repetition rate of 157 Hz.

In fact, the emission of the first peak is related to NL, as can be seen from Fig. 2, where we show the emission signals observed from an oscilloscope in (b) in response to the current pulses of 1.05 ms width applied to the sample in (a) for  $J=1.1$  and  $4.9$  A/cm<sup>2</sup>. The negative emission signal for  $J=1.1$  A/cm<sup>2</sup> implies a reduction in intensity from the

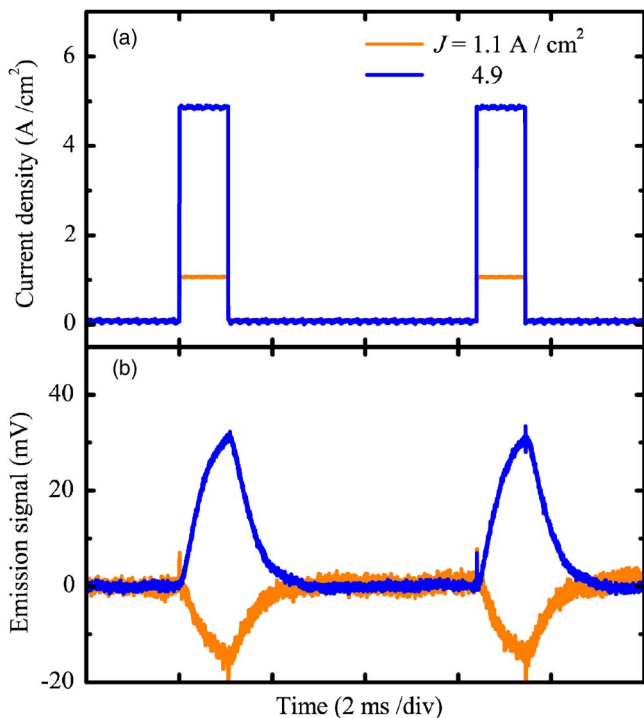


FIG. 2. (Color online) (a) The input pulses of current density of 1.05 ms width and (b) the responding emission signals for the sample, which is biased in the SDR region ( $J=1.1$  A/cm<sup>2</sup>) and in the Ohmic region ( $J=4.9$  A/cm<sup>2</sup>).

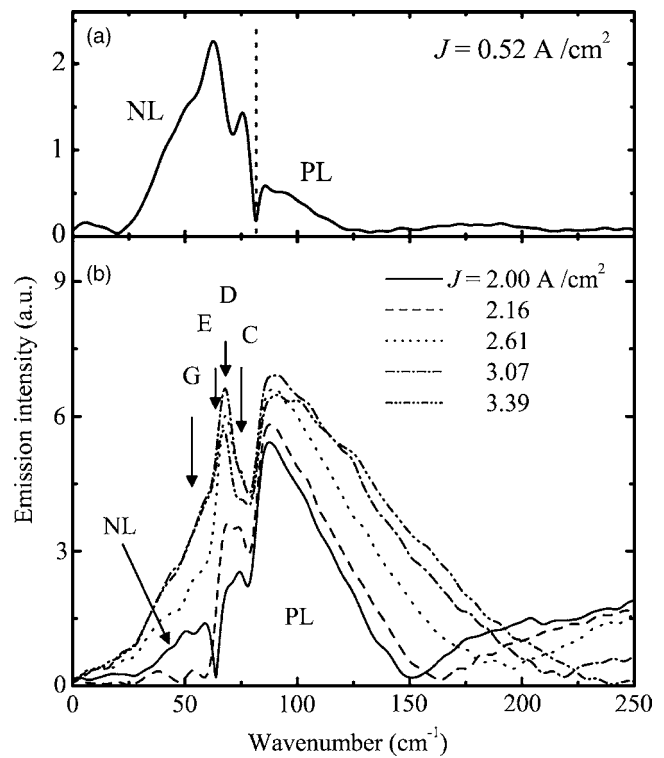


FIG. 3. Emission spectra from the sample under excitation of various current densities [ $J=0.52$  A/cm<sup>2</sup> in (a) and  $J=2, 2.16, 2.61, 3.07,$  and  $3.39$  A/cm<sup>2</sup> in (b)]. The current densities have been indicated in Fig. 1(b). The excitation pulses have a width of 2.1 ms and a repetition rate of 157 Hz.

thermal-equilibrium case ( $J=0$ ), while the positive emission signal for  $J=4.9$  A/cm<sup>2</sup> implies an increase in intensity. In agreement with the  $I$ - $J$  curve in Fig. 1(b), such a negative signal occurs at low  $J$  and reaches a maximum in magnitude at  $J=1.1$  A/cm<sup>2</sup>. For  $J>2.5$  A/cm<sup>2</sup>, the signal becomes positive and reaches the second maximum at  $J=4.9$  A/cm<sup>2</sup>.

Figure 3 shows the emission spectra for six different levels of  $J$  with a pulse width of 2.1 ms, which has been indicated in Fig. 1(b). All the spectra are measured with a resolution of 6 cm<sup>-1</sup> and using triangular apodization. For low excitation of  $J=0.52$  A/cm<sup>2</sup>, we draw a dashed line through the dip at 81.6 cm<sup>-1</sup> to separate the spectrum into two parts, as shown in Fig. 3(a). The lower-energy part is assigned to NL, while the higher-energy part to PL. The negative emission signal is associated with the difference  $I_{PL}-I_{NL}$ , where  $I_{PL}$  and  $I_{NL}$  are the areas of the PL and the NL parts, respectively. As  $J$  increases from 0, the NL part grows faster than the PL part until  $J=0.52$  A/cm<sup>2</sup>, leading to the increase of net emission intensity  $I$ , as has been shown in Fig. 1(b). With  $J$  further increasing, the NL part begins to diminish, while the PL part continues to grow. At  $J=1.5$  A/cm<sup>2</sup>,  $I_{PL} \approx I_{NL}$  and  $I \approx 0$ . For  $J>1.5$  A/cm<sup>2</sup>,  $I_{PL} > I_{NL}$ , associated with the positive emission signal. As shown in Fig. 3(b), the NL part decays to a small one with the dip shifting to 63.8 cm<sup>-1</sup> at  $J=2$  A/cm<sup>2</sup> and disappears for  $J \geq 2.16$  A/cm<sup>2</sup>. The spectra broaden in width and increase in intensity with  $J$  until the thermal quenching starts to reduce the intensity at  $J=3.39$  A/cm<sup>2</sup> at which the net intensity  $I$  and the conductivity  $\sigma$  reach their maxima.

According to the observations described above, we can give a picture of carrier transition processes involving the acceptor centers as follows. We simplify the situation to four most important levels, as illustrated in Fig. 4: (1) level  $L_0$  for

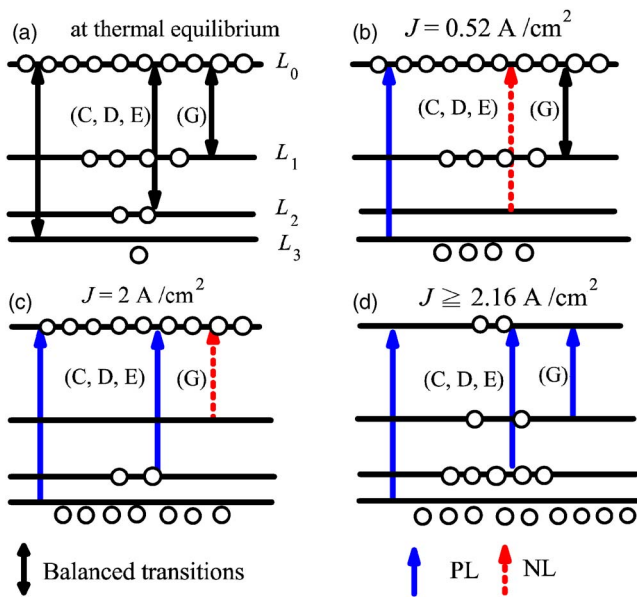


FIG. 4. (Color online) A simplified picture of carrier excitation and relaxation processes according to the previous observations. Four different situations are presented: (a) at thermal equilibrium, (b) at  $J=0.52 \text{ A/cm}^2$ , (c) at  $J=2 \text{ A/cm}^2$ , and (d) at  $J=2.16 \text{ A/cm}^2$ . Level  $L_0$  represents the ground states, level  $L_1$  represents the lowest excited states from which the transition to the ground states corresponds to the  $G$  line, level  $L_2$  represents a group of excited states from which the transition to the ground states corresponds to lines  $C$ ,  $D$ , and  $E$ , and level  $L_3$  represents the band states and the excited states very close to the band edge.

ground states, (2) level  $L_1$  for the lowest excited states from which the transition to the ground states corresponds to the  $G$  line, (3) level  $L_2$  representing a group of excited states from which the transition to the ground states corresponds to lines  $C$ ,  $D$ , and  $E$ , and (4) level  $L_3$  representing the band states and the excited states very close to the band edge. At  $J=0$ , the sample is in thermal equilibrium with the low-temperature environment. Absorption and emission of radiation are balanced, as illustrated in Fig. 4(a). When the excitation of a pulse width of 2.1 ms starts and begins to increase, residual free carriers at  $L_3$  can gain kinetic energy to remove the holes efficiently from  $L_2$  but inefficiently from  $L_1$  by impact ionization to  $L_3$ . The increase in the number of free holes at  $L_3$  causes the SNDR electrically and the PL optically due to an increase in the  $L_3$ -to- $L_0$  transition. Meanwhile, the decrease in the number of holes at  $L_2$  reduces the emission of the  $L_2$ -to- $L_0$  transition, leading to the NL of lines  $C$ ,  $D$ , and  $E$ . When the level  $L_2$  is almost empty of holes, the NL intensity reaches the maximum and the electric field  $E$  reaches the local minimum, as shown in Fig. 1. This situation occurs at  $J=0.52 \text{ A/cm}^2$ , as illustrated in Fig. 4(b). Further increasing the excitation strength will cause efficient ionization of acceptors at  $L_1$  and a further increased population of holes at  $L_3$ . Illustrated in Fig. 4(c) is the situation at  $J=2 \text{ A/cm}^2$ ,

where the level  $L_1$  is almost emptied and the level  $L_2$  is reoccupied by holes from  $L_3$  through phonon scattering. This explains the spectrum for  $J=2 \text{ A/cm}^2$  in Fig. 3(b), which has PL (but not NL) at lines  $C$ ,  $D$ , and  $E$ , and still NL at line  $G$ . For even higher levels of excitation ( $J \geq 2.16 \text{ A/cm}^2$ ), depopulation of holes at  $L_0$  by impact ionization becomes efficient. As illustrated in Fig. 4(d), there are a large number of holes at  $L_3$ , and some of them relax back to  $L_2$  and  $L_1$ . Consequently, the emission is PL and increases in intensity with  $J$  until the conductivity reaches the maximum where the thermal quenching becomes important. For narrower pulses, the thermal quenching occurs at higher  $J$ , allowing more holes to be removed from  $L_0$ . This is in agreement with the observation that the  $I$ - $J$  curve has a higher second peak for 1.05 ms pulses than for 2.1 ms ones.

In summary, PL and NL of terahertz emission from a lightly doped compensated  $p$ -type Ge under different levels of pulse excitation have been observed at cryogenic temperatures. The NL spectra appear at energies lower than the PL spectra and are attributed to the reduction in radiative transitions from excited states to the ground states. These findings may be useful for implementing terahertz emitting and cooling devices.

We thank Professor Y. W. Suen for valuable discussions and suggestions. The work was supported by National Nano Device Laboratory and National Science Council of the Republic of China under Contract No. NSC 95-2221-E-009-281.

<sup>1</sup>B. Ferguson and X. Zhang, *Nat. Mater.* **1**, 26 (2002).

<sup>2</sup>P. H. Siegel, *Int. J. High Speed Electron. Syst.* **13**, 351 (2003).

<sup>3</sup>R. Kohler, A. Tredicucci, F. Beltram, H. E. Beere, E. H. Linfield, A. G. Davies, D. A. Ritchie, R. C. Iotti, and F. Rossi, *Nature (London)* **417**, 156 (2002).

<sup>4</sup>A. Borak, S. Tsujino, C. Falub, M. Scheinert, L. Diehl, E. Müller, H. Sigg, D. Grützacher, U. Gennser, I. Sagnes, S. Blunier, T. Fromherz, Y. Campidelli, O. Kermarrec, D. Bensahel, and J. Faist, *Group-IV Semiconductor Nanostructures*, MRS Symposia Proceedings Vol. 832 (Materials Research Society, Pittsburgh, 2005), p. 69.

<sup>5</sup>A. K. Ramdas and S. Rodriguez, *Rep. Prog. Phys.* **44**, 1297 (1981).

<sup>6</sup>H.-W. Hübers, S. G. Pavlov, and V. N. Shastin, *Semicond. Sci. Technol.* **20**, S211 (2005).

<sup>7</sup>T. N. Adam, R. T. Troeger, S. K. Ray, P.-C. Lv, and J. Kolodzey, *Appl. Phys. Lett.* **83**, 1713 (2003).

<sup>8</sup>A. V. Andrianov, A. O. Zakharin, I. N. Yassievich, and N. N. Zinovev, *JETP Lett.* **79**, 365 (2004).

<sup>9</sup>C. Benoit and J. Cernogora, *Phys. Status Solidi* **11**, 295 (1965).

<sup>10</sup>T. Ashley, and G. R. Nash, and M. QinetiQ, *Mid-Infrared Semiconductor Optoelectronics, Negative Luminescence* (Springer, Berlin, 2006), Vol. 118, pp. 453–485.

<sup>11</sup>C. T. Elliott, *Philos. Trans. R. Soc. London, Ser. A* **359**, 567 (2001).

<sup>12</sup>N. Hiromoto, M. Saito, and H. Okuda, *Jpn. J. Appl. Phys., Part 1* **29**, 1739 (1990).

<sup>13</sup>A. K. Jonscher, *Proc. IEEE* **52**, 1092 (1964).

<sup>14</sup>W. Quade, G. Hüpper, E. Schöll, and T. Kuhn, *Phys. Rev. B* **49**, 13408 (1994).

<sup>15</sup>A. A. Kastalskii, *Phys. Status Solidi A* **15**, 599 (1973).